

Correlation Clustering of Organoid Images

Jannik Presberger¹ · Rashmiparvathi Keshara² · David Stein¹ ·
Yung Hae Kim² · Anne Grapin-Botton² · Bjoern Andres^{1,3}

¹TU Dresden · ²Max Planck Institute of Molecular Cell Biology and Genetics ·
³Center for Scalable Data Analytics and AI Dresden/Leipzig

Abstract

In biological and medical research, scientists now routinely acquire microscopy images of hundreds of morphologically heterogeneous organoids and are then faced with the task of finding patterns in the image collection, i.e., subsets of organoids that appear similar and potentially represent the same morphological class. We adopt models and algorithms for correlating organoid images, i.e., for quantifying the similarity in appearance and geometry of the organoids they depict, and for clustering organoid images by consolidating conflicting correlations. For correlating organoid images, we adopt and compare two alternatives, a partial quadratic assignment problem and a twin network. For clustering organoid images, we employ the correlation clustering problem. Empirically, we learn the parameters of these models, infer a clustering of organoid images, and quantify the accuracy of the inferred clusters, with respect to a training set and a test set we contribute of state-of-the-art light microscopy images of organoids clustered manually by biologists.

1	Introduction	2
2	Related work	2
3	Models	3
3.1	Correlating organoid images by partial quadratic assignment	3
3.2	Correlating organoid images by a twin network	4
3.3	Correlating organoid images by correlating their histograms	5
3.4	Clustering organoid images by correlation clustering	5
4	Algorithms	6
4.1	Inference	6
4.2	Learning	6
5	Experiments	7
5.1	Data set of organoid images with annotations	7
5.2	Correlating organoid images	7
5.3	Clustering organoid images	8
6	Conclusion	8
A	Appendix	11
A.1	Segmentation of organoids	11
A.2	Extraction of key points	11
A.3	Estimation of organoid barycenter and extent	11
A.4	Motivation of assignment costs	12
A.5	Additional qualitative experiments	12
A.6	Runtimes	12
A.7	Ethical considerations	16

arXiv:2403.13376v1 [cs.CV] 20 Mar 2024

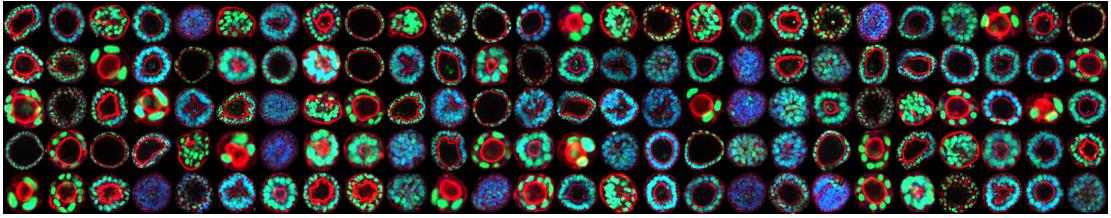


Figure 1: Depicted above are 130 images (scaled differently to the same size for illustration) of pancreatic progenitor organoids derived from human pluripotent stem cells. These organoids consist of cells expressing a nuclear Green Fluorescent Protein reporter for PDX1 (a pancreatic progenitor marker gene). After fixation, the organoids were stained with DAPI (blue) to mark the nucleus and Phalloidin (red) for F-Actin. Images were acquired using an automated spinning disc confocal microscope (20x objective of Yokogawa CV7000).

1 Introduction

Organoids are biological *in vitro* model systems used as tools to study organogenesis including morphological development, adult tissue homeostasis, function, disease manifestation, and drug discovery [25, 36, 31, 34, 29, 33]. Thanks to recent progress in organoid biology and imaging [44, 11, 17], scientists now routinely acquire light microscopy images of hundreds of organoids at once (cf. Figure 1), which reveals morphological heterogeneity in nature of biological systems. For various biological questions, it is essential to identify and classify these organoids based on their morphological characteristics [29]. Hence, scientists are faced with the task of finding patterns in the image collection, i.e., subsets of organoid images that appear similar and potentially represent the same morphological class.

In this article, we adopt mathematical models and algorithms for *correlating* organoid images, i.e., for quantifying the similarity in appearance and geometry of the organoids they depict, and for *clustering* organoid images by consolidating conflicting correlations. For correlating organoid images, we adopt two alternatives, a partial quadratic assignment problem [21] with five adjustable parameters, and a twin network [13] with 10^7 adjustable parameters. For clustering organoid images, we employ the correlation clustering problem [15] with costs defined by one or the other correlation model. Empirically, we learn the parameters of these models, infer a clustering of organoid images, and quantify the accuracy of the inferred clusters, with respect to a training set and a test set of state-of-the-art light microscopy images of organoids clustered manually by biologists. Both the data sets and the complete source code for reproducing the experiments are contributions of this article and are published as supplementary material.

2 Related work

The task of correlating images of composite objects by bringing the objects in correspondence has been studied comprehensively [14, 40, 10]. The partial quadratic assignment problem, also known as the graph matching problem [52], a relaxation of the quadratic assignment problem [32, 12], is a mathematical abstraction of this task [52, 26]. Algorithms for this NP-hard problem are an active area of computer vision research [4, 16, 1, 21, 26, 50, 51]; see [21] for a recent survey. In applications to natural images such as [14, 40, 10], one arrives at the partial quadratic assignment problem by fixing a set of key points (of one or several object models) and estimating from images annotated with key points [14, 40, 10] the appearance of key points as well as their relative location, e.g., as described in [43, 53]. In the application to organoid images, which exhibit fairly heterogeneous objects in their morphologies [19], we cannot fix the set of key points, and we do not know the object models, as we do not know the morphological classes. Instead, every image is potentially a separate organoid class. Our approach to organoid images differs from published approaches to natural images in that we fix a set of key point *classes* and an algorithm that extracts from each organoid image key points and a separate organoid model that we then match with the organoid models extracted from all other organoid images. We estimate the cost coefficients of the partial quadratic assignment problems not from key point annotations but from a clustering of an image collection. Compared to [43, 53], our object models, learning algorithm and inference algorithm are less sophisticated, but the set of object models is larger and data-dependent and gives rise to partial assignment problems with complete bipartite graphs that are hard to solve exactly.

The task of clustering images based on visual similarity is typically addressed by first estimating an embedding of single images into a metric space [9, 55], and then clustering these points by some form of metric-based clustering, e.g., *k*-means clustering. Another approach

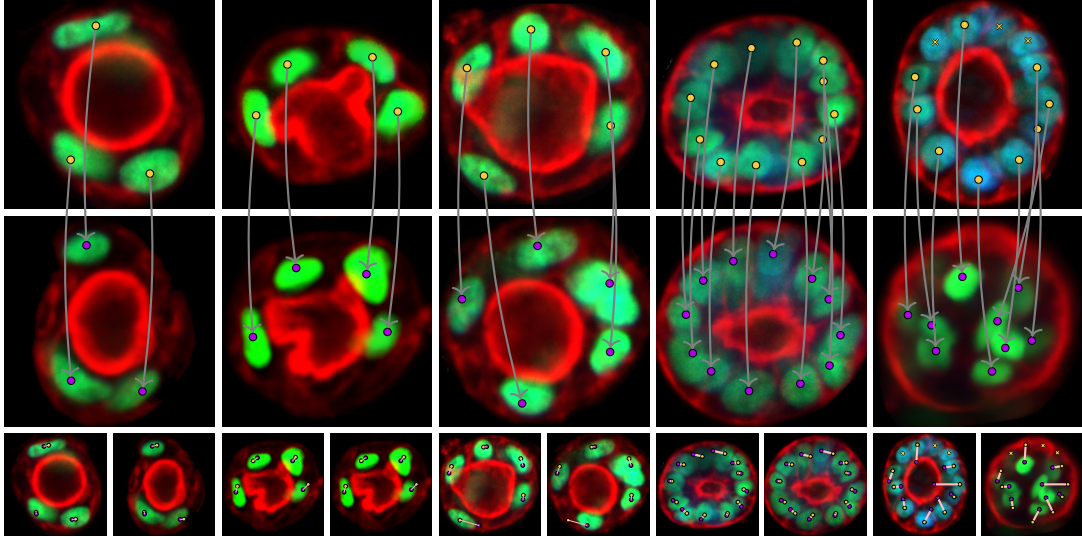


Figure 2: Depicted above, from left to right, are assignments (gray lines) between key points of five pairs of organoid images. Depicted in the bottom row are projections onto the first and the second image. Depicted in Columns 1–4 are assignments between morphologically similar organoids. Depicted in the last column is an assignment between dissimilar organoids. Note that distances between assigned key points are larger here. For illustration, images are rotated, and only key points of cell nuclei are shown.

to clustering images is to first estimate a map from any *pair* of images to a real number that is positive for images in the same cluster and negative for images in distinct clusters (at loss zero), and to then cluster a set of images by correlation clustering [8, 15]. Examples of this approach include [24, 45, 37]. A combination of both approaches is introduced in [3]. One reason why forensics researchers [45, 37] and also we here adopt the correlation clustering problem is its unbiasedness with respect to clusterings a priori [28, 5, 6]. Thanks to recent progress [3, 27, 2, 54, 47] toward algorithms for the NP-hard correlation clustering problem and the closely related clique partition problem and multicut problem, some instances not accessible previously can now be solved exactly; see [48, 49] for recent benchmarks.

The task of extracting images of individual organoids from microscopy images of numerous organoids within a field of view is referred to as organoid segmentation [41]. The images of individual organoids we contribute as supplementary material are extracted from microscopy images using [46] as we describe in Appendix A.1. The task of organoid tracking [38] is not addressed in this article.

3 Models

3.1 Correlating organoid images by partial quadratic assignment

The first idea we pursue in order to compare one image of a first organoid to another image of a second organoid is to assign points in the first image to points in the second image such that the images appear similar at assigned points, and such that the assignments of any two pairs of points are geometrically consistent. This idea is made rigorous below and is illustrated in Figure 2.

Feasible solutions We consider a finite collection J of organoid images. From any image $j \in J$, we extract a finite set V_j of key points as described in Appendix A.2. For any pair $j, k \in J$ of distinct images, we call a relation between V_j and V_k a *feasible assignment* if and only if any point in V_j is related to at most one point in V_k , and any point in V_k is related to at most one point in V_j . We encode any feasible assignment by the vector $x \in \{0, 1\}^{V_j \times V_k}$ such that for any point $v \in V_j$ and any point $w \in V_k$, we have $x_{vw} = 1$ if and only if v is assigned to w . The set $X_{V_j V_k}$ of the encoding vectors of all feasible assignments is written below, with the above conditions expressed equivalently in the form of linear inequalities.

$$X_{V_j V_k} = \left\{ x \in \{0, 1\}^{V_j \times V_k} \mid \forall v \in V_j: \sum_{w \in V_k} x_{vw} \leq 1 \text{ and } \forall w \in V_k: \sum_{v \in V_j} x_{vw} \leq 1 \right\}$$

Partial quadratic assignment problem For any images $j, k \in J$ and any points $v \in V_j$ and $w \in V_k$, we define below a cost $c_{vw}^{jk} \in \mathbb{R}$ that is negative if the point v in the image j appears similar to the point w in the image k , and positive if the images appear dissimilar at these points.

For any distinct points $v, v' \in V_j$ and any distinct points $w, w' \in V_k$, we also define below a cost $c_{vv'w'w}^{jk} \in \mathbb{R}$ that is negative if the assignment of the point v in the image j to the point w in the image k is geometrically consistent with the assignment of the point v' in the image j to the point w' in the image k , and positive otherwise. For any feasible solution $x \in X_{V_j V_k}$, we define its cost $\varphi_{c^{jk}}(x) \in \mathbb{R}$ as

$$\begin{aligned} \varphi_{c^{jk}}(x) = & \frac{1-\lambda}{n_1^{jk}} \sum_{v \in V_j} \sum_{w \in V_k} c_{vw}^{jk} x_{vw} \\ & + \frac{\lambda}{n_2^{jk}} \sum_{v \in V_j} \sum_{v' \in V_j \setminus \{v\}} \sum_{w \in V_k} \sum_{w' \in V_k \setminus \{w\}} c_{vv'w'w}^{jk} x_{vw} x_{v'w'} \end{aligned} \quad (1)$$

with the constants $n_1^{jk} := \min\{|V_j|, |V_k|\}$ and $n_2^{jk} := \binom{n_1^{jk}}{2}$ and a model parameter $\lambda \in (0, 1)$. Note: The cost $c_{vv'w'w}^{jk}$ is payed if and only if $x_{vw} = x_{v'w'} = 1$, i.e., if the point v is assigned to the point w , and the point v' is assigned to the point w' . Now, the task of finding a feasible assignment of minimum cost takes the form of the partial quadratic assignment problem

$$\min \{ \varphi_{c^{jk}}(x) \mid x \in X_{V_j V_k} \} . \quad (2)$$

Cost coefficients For any organoid image $j \in J$ and any point $v \in V_j$ in the image, we let $a_v^j \in \mathbb{R}^3$ denote the vector of the three color channels of the image j at the point v . We measure the similarity in appearance of a point $v \in V_j$ in an image j and a point $w \in V_k$ in an image k by the metric $d_{vw} := |a_v^j - a_w^k|$.

For any image $j \in J$, we estimate the barycenter $r_0^j \in \mathbb{R}^2$ of the organoid in the image plane, as well as the extent $\sigma_0^j \in \mathbb{R}^+$ of the organoid, i.e., the furthest l_2 -distance of any point of the organoid from its barycenter, as described in Appendix A.3. For any point $v \in V_j$, we consider its coordinates $r_v^j \in \mathbb{R}^2$ in the image plane, as well as the distance between r_v^j and the barycenter, relative to the extent of the organoid, i.e., $\sigma_v^j := |r_v^j - r_0^j|/\sigma_0^j$. For any pair of points $v, v' \in V_j$, we consider the angle $\alpha_{vv'}^j := \angle(r_v^j - r_0^j, r_{v'}^j - r_0^j)$. For any pair of images $j, k \in J$, any point $v \in V_j$ and any point $w \in V_k$, we define $d_{vw}^j := |\sigma_v^j - \sigma_w^k|$. For any pair of images $j, k \in J$, any distinct points $v, v' \in V_j$ and any distinct points $w, w' \in V_k$, we define $d_{vv'w'w}^{jk} := |\alpha_{vv'}^j - \alpha_{w'w}^k|$. We justify these definitions in Appendix A.4.

With model parameters $\delta, \delta', \delta'' \in \mathbb{R}^+$ and $\theta \in (0, 1)$, we define the coefficients in (1) as

$$c_{vw}^{jk} := \theta (d_{vw} - \delta) + (1 - \theta) (d_{vw}^j - \delta') \quad (3)$$

$$c_{vv'w'w}^{jk} := d_{vv'w'w}^{jk} - \delta'' . \quad (4)$$

According to these definitions, distances $d_{vw}, d_{vw}^j, d_{vv'w'w}^{jk}$ greater than the respective thresholds $\delta, \delta', \delta''$ result in positive costs associated with the assignments of v to w and v' to w' . Distances less than the thresholds result in negative costs (i.e., rewards) associated with these assignments.

Normalization For any pair of images $j, k \in J$ and the costs $\varphi_{c^{jk}}(x^{jk})$ and $\varphi_{c^{kj}}(x^{kj})$ of solutions x^{jk} and x^{kj} to the instances of the partial quadratic assignment problems between these images, we consider the real number

$$\phi_{\{j,k\}} := - \frac{\min \{ \varphi_{c^{jk}}(x^{jk}), \varphi_{c^{kj}}(x^{kj}) \}}{(1-\lambda)(\theta\delta + (1-\theta)\delta') + \lambda\delta''} . \quad (5)$$

In (5), the minimum merely serves the purpose of defining $\phi_{\{j,k\}}$ by a form that is invariant under transposition of j and k . In theory, $\varphi_{c^{jk}}(x^{jk}) = \varphi_{c^{kj}}(x^{kj})$ because the partial quadratic assignment problem and the cost function we define for this problem are invariant under transposition of j and k . Also in (5), the denominator is a normalizing constant that only depends on model parameters. As we show in Appendix A.4, the number $\phi_{\{j,k\}}$ is confined to the interval $[0, 1]$ and is *comparable across instances* of the partial quadratic assignment problem.

3.2 Correlating organoid images by a twin network

The second idea we pursue in order to compare one image of a first organoid to another image of a second organoid is to learn from a collection of organoid images clustered by biologists a map from any *pair* of organoid images to a real number that is positive for images in the same cluster and negative for images in distinct clusters (at loss zero).

To this end, we scale every organoid image to fit into a grid of $n \cdot n$ pixels, with $n = 256$, centered and padded with zeroes in case the image is not square. For any organoid image $j \in J$,

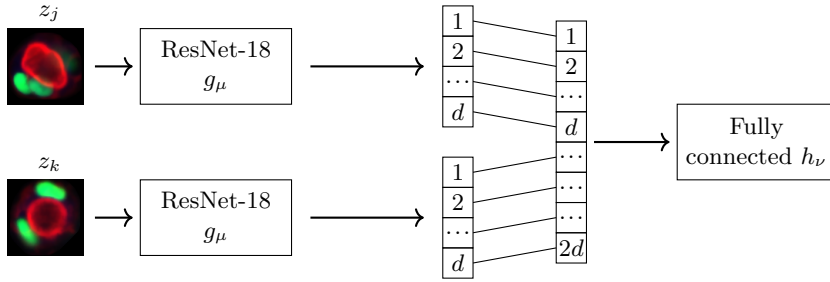


Figure 3: In order to map a pair of scaled organoid images $z_j, z_k \in \mathbb{R}^{3n^2}$ to a real number that is supposed to be positive for images in the same cluster and negative for images in distinct clusters, we learn a twin network consisting of a head $g_\mu: \mathbb{R}^{3n^2} \rightarrow \mathbb{R}^d$ in the form of a ResNet-18 [22] with $d = 128$ and adjustable parameters $\mu \in \mathbb{R}^{11,242,176}$, and a base $h_\nu: \mathbb{R}^d \times \mathbb{R}^d \rightarrow \mathbb{R}$ in the form of one fully connected hidden layer and one output node, with adjustable parameters $\nu \in \mathbb{R}^{33,025}$.

we let $z_j \in \mathbb{R}^{3n^2}$ denote the vector of the intensities of the three color channels of all pixels in the scaled image. For any distinct organoid images $j, k \in J$, we let z_{jk} denote the concatenation of z_j and z_k . We define a function that maps any z_{jk} to a real number that is supposed to be positive for images in the same cluster and negative for images in distinct clusters. This function has the form of the twin network [13] depicted in Figure 3. It consists of a head $g_\mu: \mathbb{R}^{3n^2} \rightarrow \mathbb{R}^d$ in the form of a ResNet-18 [22] with $d = 128$ and adjustable parameters $\mu \in \mathbb{R}^{11,242,176}$, and a base $h_\nu: \mathbb{R}^d \times \mathbb{R}^d \rightarrow \mathbb{R}$ in the form of one fully connected hidden layer and one output node, with adjustable parameters $\nu \in \mathbb{R}^{33,025}$. Overall, this twin network defines a function $\tau_\theta: \mathbb{R}^{6n^2} \rightarrow \mathbb{R}$ with adjustable parameters $\theta := (\mu, \nu)$ such that for any pair of organoid images $j, k \in J$, we have $\tau_\theta(z_{jk}) = h_\nu(g_\mu(z_j), g_\mu(z_k))$.

3.3 Correlating organoid images by correlating their histograms

A third idea we pursue in order to compare one image of a first organoid to another image of a second organoid is to compare the histograms of these images.

To this end, we define a twin network analogous to the one described in Section 3.2 and depicted in Figure 3, except that here, the input consists of the histograms $h_j, h_k \in \{0, \dots, 255\}^3$ of two images $j, k \in J$. The head of this twin network has the form of a ResNet-18 [22] with $d = 128$, one-dimensional convolutions and adjustable parameters $\mu' \in \mathbb{R}^{3,910,464}$. The base has exactly the form described in Section 3.2, with adjustable parameters $\nu' \in \mathbb{R}^{33,025}$. We write $\theta' = (\mu', \nu')$ for the parameters of this network and write $\tau_{\theta'}$ for the function defined by this network.

A fourth idea we implement as a baseline in order to compare two images of organoids by comparing their histograms is to compute the Hellinger distance [23] between these histograms.

3.4 Clustering organoid images by correlation clustering

The idea we pursue in order to cluster a collection J of organoid images is to consider for any distinct images $j, k \in J$ a cost $q_{\{j,k\}} \in \mathbb{R}$ that is positive for images of similar organoids and negative for images of dissimilar organoids, and to search for a partition (clustering) of the set J that minimizes the sum of costs of those pairs of images that are in distinct clusters.

Feasible solutions We consider as feasible solutions all partitions of the set J of organoid images. We encode any partition Π of J by the vector $y: \binom{J}{2} \rightarrow \{0, 1\}$ such that for any pair $\{j, k\} \in \binom{J}{2}$ of distinct images, we have $y_{\{j,k\}} = 1$ if and only if j and k are in distinct clusters, i.e., if $\forall U \in \Pi: \{j, k\} \not\subseteq U$. The set Y_J of the encoding vectors of all partitions is written below, with transitivity expressed in the form of linear inequalities.

$$Y_J = \left\{ y: \binom{J}{2} \rightarrow \{0, 1\} \mid \forall j \in J \forall k \in J \setminus \{j\} \forall l \in J \setminus \{j, k\}: y_{\{j,l\}} \leq y_{\{j,k\}} + y_{\{k,l\}} \right\}$$

Correlation clustering problem For any pair of distinct images $j, k \in J$, we define below a cost $q_{\{j,k\}} \in \mathbb{R}$ associated with j and k being in distinct clusters. For any feasible solution $y \in Y_J$, we define its cost $\xi_q(y) \in \mathbb{R}$ as

$$\xi_q(y) = \sum_{\{j,k\} \in \binom{J}{2}} q_{\{j,k\}} y_{\{j,k\}}. \quad (6)$$

Hence, the task of finding an optimal partition of the image collection J assumes the form of the correlation clustering problem

$$\min \{\xi_q(y) \mid y \in Y_J\} . \quad (7)$$

Note: The number, size and size ratio of clusters is neither constrained nor assigned a cost explicitly in this problem. Instead, these properties are determined by its solutions.

Cost coefficients We consider four alternatives of defining the cost $q_{\{j,k\}}$ associated with a pair of distinct images $j, k \in J$ being in distinct clusters, one for each method we consider for correlating organoid images:

When correlating organoid images by partial quadratic assignment, as described in Section 3.1, we define $q_{\{j,k\}} := \phi_{\{j,k\}} - \delta'''$, with an additional model parameter $\delta''' \in [0, 1]$. When correlating organoid images by a twin network τ_θ , as described in Section 3.2, we define $q_{\{j,k\}} := \frac{1}{2}(\tau_\theta(z_{jk}) + \tau_\theta(z_{kj}))$. When correlating organoid images j and k via their histograms h_j and h_k by a twin network $\tau'_{\theta'}$, as described in Section 3.3, we define $q_{\{j,k\}} := \frac{1}{2}(\tau'_{\theta'}(h_{jk}) + \tau'_{\theta'}(h_{kj}))$ with h_{jk} the concatenation of the histograms h_j and h_k . When correlating organoid images j and k via their histograms h_j and h_k by the Hellinger distance $d_H(h_j, h_k)$, as described in Section 3.3, we define $q_{\{j,k\}} := 1 - d_H(h_j, h_k) - \delta'''$, with an additional model parameter $\delta''' \in [0, 1]$.

4 Algorithms

4.1 Inference

Partial quadratic assignment problem We search for feasible solutions to the instances defined in Section 3.1 of the partial quadratic assignment problem by means of a local search algorithm that exploits the geometry of these instances:

For any two images $j, k \in J$, we assume (hypothetically) that a geometrically consistent feasible assignment $x \in X_{V_j V_k}$ as defined in Appendix A.4 exists and consider the transformation of the image plane defined by x according to Definition 1. This transformation is composed of a translation, a rotation and a scaling. We estimate the translation from the estimates of the barycenters of the organoids. We estimate the scaling from the estimates of the extents of the organoids. For any rotation angle γ , we thus obtain one transformation f_γ .

For any angle $\gamma \in \{\frac{2\pi n}{N}\}_{n \in \{0, \dots, N-1\}}$, we construct a feasible assignment $x^\gamma \in X_{V_j V_k}$ as follows: For any $v \in V_j$, we constrain the set of candidates to a subset $V_{jk} \subseteq V_k$ of cardinality $|V_{jk}| = \lfloor |V_k|/M \rfloor$ for which $\sum_{w \in V_{jk}} \|f_\gamma(r_v^j) - r_w^k\|_2$ is minimal. Starting from $x = 0$, we greedily assign pairs of unassigned points $v \in V_j$ and $w \in V_{jk}$ for which switching x_{vw}^γ to one reduces $\varphi_{c^{jk}}(x^\gamma)$ maximally, until even the best additional assignment would increase $\varphi_{c^{jk}}(x^\gamma)$. We output x^γ for a γ that minimizes $\varphi_{c^{jk}}(x^\gamma)$. In our experiments, $N = 75$ and $M = 10$.

Correlation clustering problem We solve globally all instances of the correlation clustering problem for our quantitative experiments, by separating precisely the inequalities from the definition of Y_J in the integer linear programming procedure of Gurobi [20]. We solve locally the instances of the correlation clustering problem for our qualitative experiments in Appendix A.5, by means of [30, Algorithm 2].

4.2 Learning

Partial quadratic assignment problem In order to learn the parameters $\delta, \delta', \delta'', \theta, \lambda$ of the instances defined in Section 3.1 of the partial quadratic assignment problem, as well as the parameter δ''' , we classify pairs of organoid images j and k independently as being of the same organoid class, if $\phi_{\{j,k\}} \geq \delta'''$, and of distinct organoid classes, if $\phi_{\{j,k\}} < \delta'''$. Our learning objective is to minimize the F_1 score of this classification with respect to all pairs of distinct images of the training set, and the decisions by biologists whether the images belong to the same cluster or distinct clusters. We perform this minimization locally, by simulated annealing: In Iteration $t = 0$, we initialize the parameters, solve all $\binom{|J|}{2}$ assignment problems locally, as described in Section 4.1, classify pairs of images independently, as described above, and compute the F_1 score $F_1^{(0)}$. In every successive iteration t , we draw for every parameter a number u from a normal distribution with zero mean and standard deviation $\kappa \in \mathbb{R}$, add u to that parameter, solve all $\binom{|J|}{2}$ assignment problems locally, as described in Section 4.1, classify pairs of images independently and compute the F_1 score $F_1^{(t)}$. If $F_1^{(t)} > F_1^{(t-1)}$, we accept the parameter update. Otherwise, we accept the parameter update with probability $e^{(F_1^{(t)} - F_1^{(t-1)})/T_t}$, where $T_t \in \mathbb{R}^+$ is called the temperature at iteration t that we adjust according to a geometric cooling schedule $T_t = \beta \cdot T_{t-1}$. If the parameter update is revoked we maintain $F_1^{(t)} := F_1^{(t-1)}$. After an iteration limit t_{max} is reached, we output parameters for which the F_1 score is maximal over all iterations.

In our experiments, we start with $\delta = \delta' = \delta'' = 0.2$, $\lambda = \theta = 0.5$, $T_0 = 0.3$ and fix $\kappa = 0.1$, $\beta = 0.99$, $t_{max} = 140$ (8 hours).

Twin network In order to learn the parameters θ of the twin network τ_θ , our objective is to minimize the logistic loss with respect to all pairs of distinct images of the training set, and the decisions by biologists whether the images belong to the same cluster or distinct clusters. In our experiments, we solve this problem locally, by means of stochastic gradient descent, with an adaptive learning rate. More specifically, we employ AdamW [35] with mini-batches, each consisting of 64 pairs of images, 32 pairs where both images are from the same cluster, and 32 pairs where the two images are from distinct clusters. The initial learning rate is 10^{-4} . The number of iterations is 6000. Optionally, for data augmentation, we apply the following transformations to images, each with a probability of $\frac{1}{5}$, independently: Reflection about the horizontal axis, reflection about the vertical axis, rotation about the origin by an angle drawn uniformly at random from $[0, 2\pi)$. In order to learn the parameters θ' of the twin network $\tau_{\theta'}$, the procedure is exactly analogous, except that we do not augment histograms.

Hellinger Distance In order to estimate the threshold $\delta''' \in [0, 1]$ on the Hellinger Distance, we classify pairs of organoid images j and k independently as being of the same organoid class, if $d_H(h_j, h_k) \leq 1 - \delta'''$, and of distinct organoid classes, if $d_H(h_j, h_k) > 1 - \delta'''$. Our learning objective is to maximize the F_1 score of this classification with respect to a training set of organoid images clustered manually by biologists. We perform this maximization by exhaustive search over all $\delta''' \in \{\frac{n}{N'}\}_{n \in \{0, \dots, N'\}}$ with $N' = 100$.

5 Experiments

5.1 Data set of organoid images with annotations

We report below on experiments with respect to four sets of organoid images that we refer to as *Train-100*, *Test-100*, *Test-30* and *Unlabeled-1000* (see Figures 1 and 6 and Appendix A.5). Each of these sets consists of light microscopy images of individual organoids we have extracted from larger images by means of [46], as described in Appendix A.1. *Train-100* and *Test-100* each contain 10 organoid images of each of 10 distinct organoid classes identified by biologists based on the appearance of organoids in the image collection. *Test-30* contains another 10 images of each of 3 additional organoid classes not contained in *Train-100* or *Test-100*. We use *Train-100* exclusively for learning. We use *Test-100* for measuring the accuracy of the classification of image pairs and of the clustering of images, with respect to a set of images not seen during learning, of organoid classes seen during learning. We use *Test-30* for measuring the accuracy with respect to a set of images not seen during learning, of organoid classes not seen during learning. We use *Unlabeled-1000* for reporting qualitatively in Appendix A.5 the clustering on an unlabeled set of 1000 images of organoids of unknown classes. All four sets of organoid images are included as supplementary material, along with the annotations of the first three.

5.2 Correlating organoid images

Toward the classification of pairs of organoid images as belonging to the same or distinct clusters, we proceed in two steps: Firstly, we learn the models defined in Sections 3.1 to 3.3 from the set *Train-100* by the algorithms described in Section 4.2. Secondly, we apply these learned models in order to infer independently for pairs of images whether the images belong to the same or distinct clusters, for the sets *Test-100*, *Test-30* and the combined set *Test-100/30*, by the algorithms described in Section 4.1. We report in Table 1 and Figure 4 (left) how close these classifications are to classifications by biologists, on images not seen during learning, of organoid classes seen during learning (*Test-100*), organoid classes not seen during learning (*Test-30*) and a combination of both (*Test-100/30*).

It can be seen from Table 1 that the accuracy is above 90% for all models, for organoid classes seen during learning (*Test-100*). The accuracy is lower, about 70%-80% depending on the model, for organoid classes not seen during learning (*Test-30*). The accuracy is between these numbers for pairs of organoid images where one image is from a class seen during learning, and the other is not. Closest to the truth by an accuracy of 98.9% and 82.1% on *Test-100* and *Test-30*, respectively, are the classifications by the twin network learned with data augmentation. The partial quadratic assignment problem is the most accurate model (92.8%) for separating the organoid images in *Test-100* from those in *Test-30*. It is also the least accurate model (71.3%) on *Test-30*. From the left column of Figure 4, we see: With respect to cuts, all models are accurate. With respect to joins, both the twin network learned on cumulative histograms as well as the Hellinger distance are almost uninformative, while the other models are informative. With respect to *Test-100*, the twin network is the most accurate model across all metrics. With

respect to Test-30, the partial quadratic assignment problem has a higher recall of joins and precision of cuts, by a margin of 9.6% and 2.3%, respectively. At the same time, the twin network has a higher precision of joins and recall of cuts, by a margin of 16.8% and 20%, respectively. Computation times are discussed in Appendix A.6.

5.3 Clustering organoid images

Toward the clustering of organoid images, we solve the instances of the correlation clustering problem defined in Section 3.4 by the algorithm described in Section 4.1. We report in Table 1, Figure 4 (right) and Figure 6 how close these clusterings are to clusterings by biologists, on images not seen during learning, of organoid classes seen during learning (Test-100), organoid classes not seen during learning (Test-30) and a combination of both (Test-100/30). We report in Figure 5 how this distance between computed and true clusterings is affected by a constant added to all costs of the correlation clustering problem. We discuss computation times in Appendix A.6.

Closest to the truth for Test-100 by a variation of information [7, 39] of 0.14 is the twin network learned with data augmentation. For these images, it is consistently better than the other models with respect to all reported metrics. Closest to the truth for Test-30 by a variation of information of 0.79 is the partial quadratic assignment problem. It generalizes better from the classes of organoids seen during learning (Train-100 and Test-100) to the classes of images not seen during learning and contained in Test-30. Comparing the accuracy of clustering and classification by comparing Rand’s index (RI) [42] with accuracy (ACC) in Table 1, we observe: For Test-100, consolidating conflicting independent classifications of pairs of images by solving the correlation clustering problem increases the accuracy consistently, for all models. For Test-30, it increases the accuracy for the partial quadratic assignment problem and the Hellinger Distance while decreasing it for the twin networks. It can be seen from Figure 5 that adding a constant to all costs of the correlation clustering problem determined by partial quadratic assignment does not improve solutions on any of the test sets. In contrast, adding a positive constant to the costs determined by the twin network improves solutions on Test-30.

6 Conclusion

For the light microscopy images of organoids we have considered in this study, it can be seen from the experiments that both the partial quadratic assignment problem and the twin network can be applied, together with correlation clustering, to partition an image collection in a way that is similar to a partition of the same collection by biologists, by a Rand Index of 97.2% and 99.4%, respectively, for classes of organoids seen during training, and by a Rand Index of 77.2% and 80.2%, respectively, for classes of organoids not seen during training. This enables unbiased quantification of heterogeneity and identification of morphological parameters of emerging patterns in biological systems. This result cannot be considered a fully automatic solution to the problem but can be considered an informative proposal for computer-assisted clustering of organoid images. Quantifying the amount of work it can save compared to a fully manual

Test data	Model	Classification of pairs					Correlation clustering									
		ACC	PC	RC	PJ	RJ	RI	VI	VI _C	VI _J	PC	RC	PJ	RJ	F _{1C}	F _{1J}
100	PQAP	95.0	97.7	96.8	70.7	77.1	97.2	0.68	0.53	0.15	97.7	99.3	92.0	76.7	98.5	83.7
	TNIa	98.9	99.6	99.2	92.5	95.8	99.4	0.14	0.09	0.05	99.6	99.8	97.7	96.0	99.7	96.9
	TNI	92.6	99.0	98.4	84.7	89.8	98.2	0.38	0.18	0.20	99.1	98.9	89.5	91.3	99.0	90.4
	TNH	92.6	96.6	95.2	58.0	66.7	93.0	1.58	0.92	0.67	96.0	96.3	62.0	59.8	96.2	60.9
	d_H	90.1	95.1	93.9	46.0	51.8	91.6	1.76	1.19	0.57	95.1	95.8	54.2	50.2	95.4	52.1
30	PQAP	71.3	91.1	64.7	52.3	85.9	77.2	0.79	0.16	0.63	95.9	70.0	58.3	98.3	80.9	73.2
	TNIa	82.1	88.8	84.7	69.1	76.3	80.2	1.16	0.72	0.44	86.1	85.0	67.6	69.6	85.6	68.6
	TNI	78.4	89.3	78.0	61.8	79.3	72.9	1.20	0.60	0.59	85.3	73.3	54.8	71.9	78.9	62.2
	TNH	78.9	83.8	86.0	66.9	63.0	77.5	1.49	1.01	0.48	81.4	87.3	66.4	55.6	84.2	60.5
	d_H	75.4	85.1	78.0	58.9	69.6	78.6	1.31	0.74	0.58	84.4	84.7	65.6	65.2	84.5	65.4
100/30	PQAP	92.8	100.0	92.8	0.0	-	94.8	1.24	0.64	0.60	97.8	96.7	61.5	70.6	97.2	65.8
	TNIa	91.1	100.0	91.1	0.0	-	95.3	0.88	0.27	0.61	99.2	95.8	61.2	89.2	97.4	72.6
	TNI	90.7	100	90.7	0.0	-	94.7	1.09	0.38	0.72	98.7	95.5	58.3	83.1	97.1	68.5
	TNH	90.1	100.0	90.1	0.0	-	92.0	2.13	1.05	1.08	96.6	94.8	44.1	54.9	95.7	48.9
	d_H	85.9	100.0	85.9	0.0	-	90.3	2.62	1.44	1.19	95.9	94.0	33.9	40.7	94.8	37.0

Table 1: We report above how close *classifications* of pairs of organoid images and *clusterings* of organoid images are to decisions by biologists, on images not seen during training, of organoid classes seen during training (Test-100), organoid classes not seen during training (Test-30) and a combination (Test-100/30). We compare the partial quadratic assignment problem (PQAP), the twin networks for images with and without data augmentation (TNI, TNIa), the twin networks for histograms (TNH) and the Hellinger distance (d_H). We abbreviate the accuracy (ACC), precision (P), recall (R), cuts (C), joins (J), Rand’s index (RI), variation of information (VI) and F₁-score (F₁).

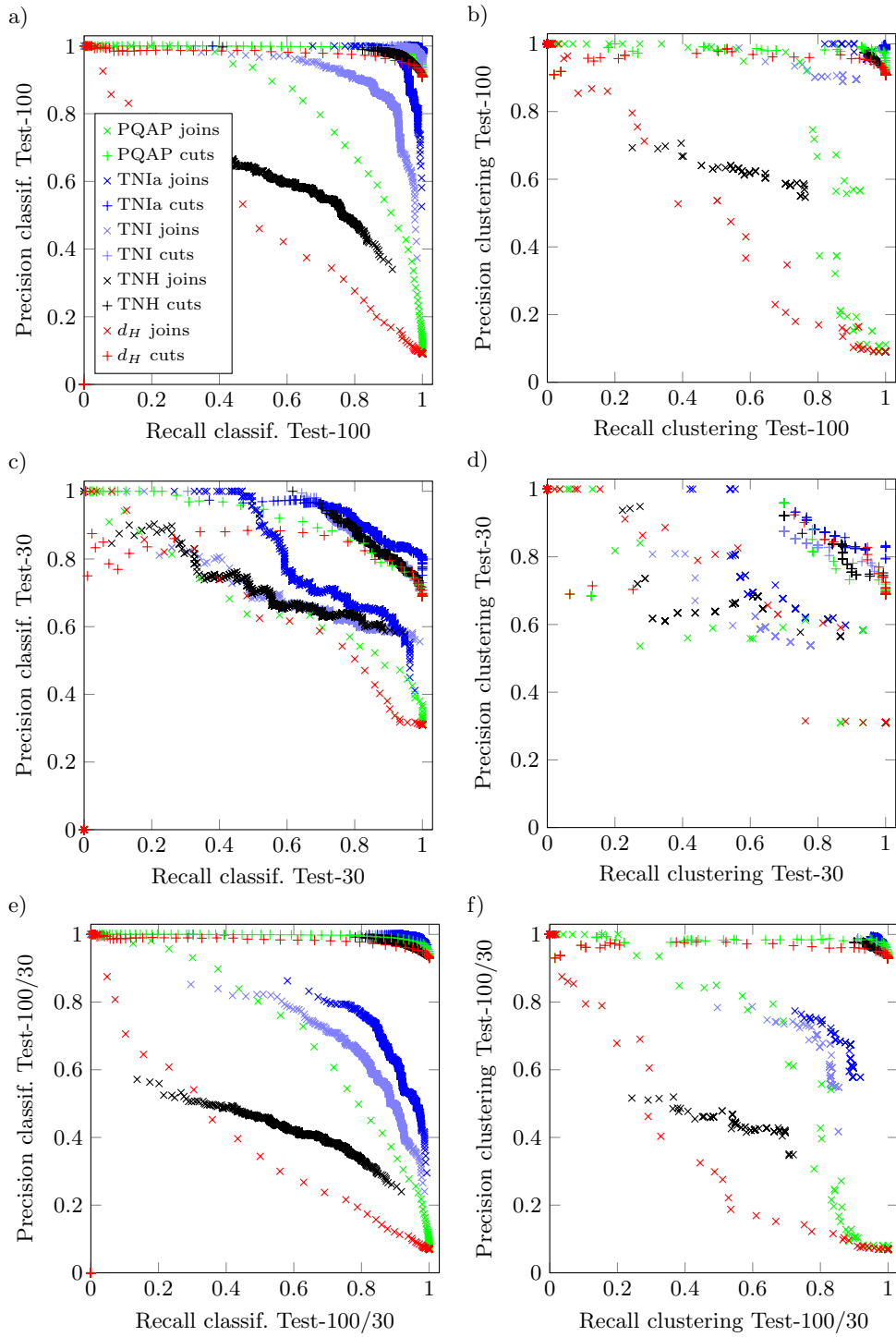


Figure 4: Depicted above are precision recall curves for the independent classification of pairs of organoid images (left) and the clustering of organoid images (right), on the data sets Test-100 (top), Test-30 (middle) and Test-100/30 (bottom).

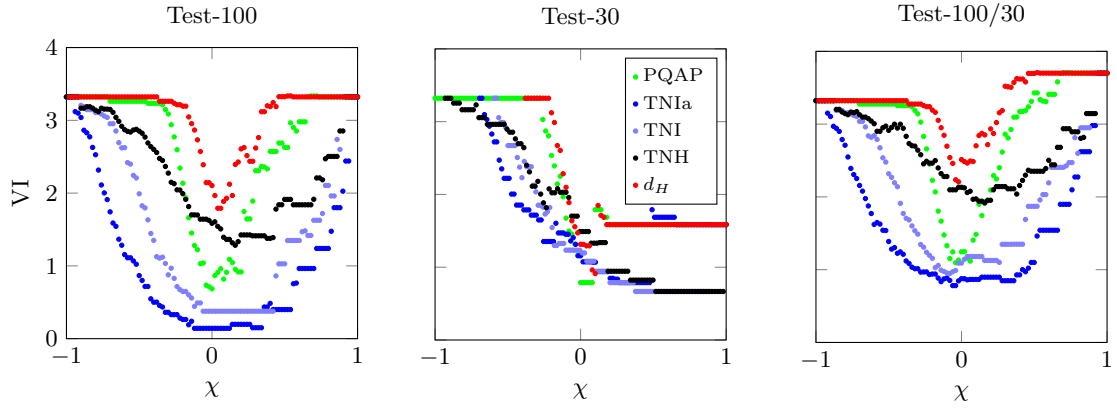


Figure 5: Depicted above is the variation of information distance between computed and true clusterings of organoid images as a function of a constant χ added to all cost coefficients of the correlation clustering problem. For this comparison, the costs from both the PQAP and the twin networks are scaled globally (not per instance) to $[-1, 1]$, which does not alter the solutions.

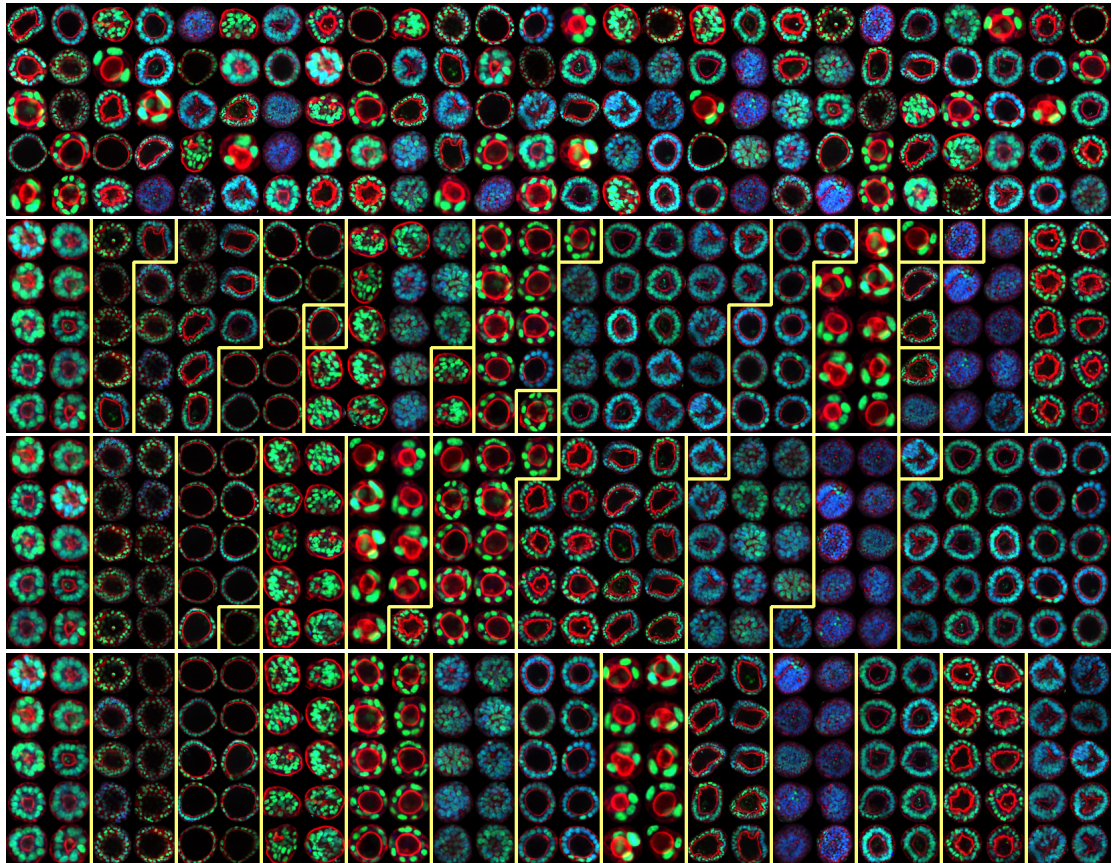


Figure 6: Depicted above are, in Row 1, all organoid images of the sets Test-100 and Test-30 (scaled differently to the same size for illustration), in Row 2, the clustering of the images wrt. costs defined by the partial quadratic assignment problem, in Row 3, the clustering of the images wrt. costs defined by a twin network, and in Row 4, the clustering by biologists of Test-100 (Clusters 1–10) and Test-30 (Clusters 11–13).

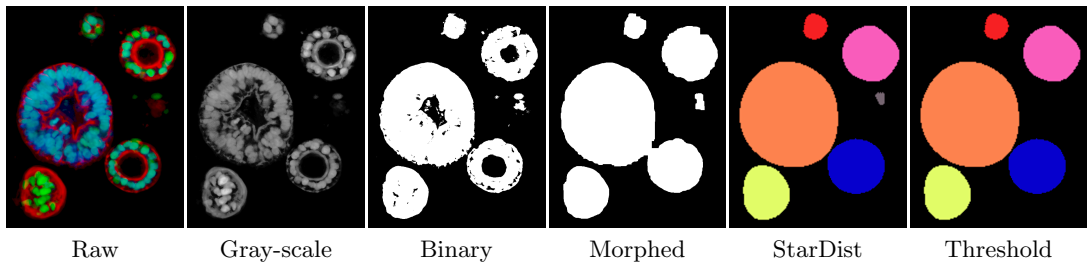


Figure 7: Image pre-processing and organoid segmentation

clustering of organoid images is one direction of future research that connects with the field of human computer interaction. Our study is limited to 2-dimensional light microscopy images of organoids. Generalizations to 3-dimensional images, also electron microscopy images, and possibly even sequences of such images can be considered in principle but are not discussed here. Toward computer vision methods with potential for applications beyond organoid images, we have introduced a normalization that makes solutions to the partial quadratic assignment problem comparable across instances. We contribute the organoid images with annotations as well as the instances from this application of the NP-hard partial quadratic assignment problem and correlation clustering problem some of which are challenging even for the most sophisticated algorithms. The source code of all algorithms and for reproducing the experiments is provided as supplementary material. Ethical considerations are discussed in Appendix A.7.

Acknowledgements Organoids were cultured in Organoid and Stem Cell Facility, and experiments in 384-well plates and image acquisitions were performed with the support of the in-house screening facility (Technology Development Studio) of the Max Planck Institute of Molecular Cell Biology and Genetics. B.A. is supported by the Center of Scalable Data Analytics and AI, Dresden/Leipzig. A.G.B. and Y.H.K. are supported by the Max Planck Society. R.K. is supported by the Deutsche Forschungsgemeinschaft (DFG, German Research Foundation), Project 288034826-IRTG 2251 (to A.G.B.).

A Appendix

A.1 Segmentation of organoids

In order to extract images of individual organoids from microscopy images of numerous organoids within a field of view, we apply the StarDist method [46]. Before applying StarDist, we process the images as depicted in Figure 7 and described below. For further details, we refer to the source code. Firstly, we convert the raw images with three color channels to gray-scale images. Secondly, we binarize the gray-scale images by applying a threshold. Thirdly, in order to remove noise while preserving the shapes and boundaries of the organoids, we apply a sequence of morphological operations. The morphed images are then put into the StarDist method that outputs segments. We suppress small segments.

A.2 Extraction of key points

For every organoid image j , we construct a set V_j of key points as described below. These key points are supposed to describe the organoid.

The green and the blue color channel show nuclei of cells within the organoid. We construct key points for these channels independently, as the brightness of nuclei in these channels is different. To each channel, we apply the StarDist method [46] that outputs segments. For each segment, we introduce one key point $v \in V_j$ at the barycenter r_v^j of the segment and associate with this key point the average color a_v^j across the segment.

The red color channel shows membranes within the organoid. For this channel, we construct key points in a greedy manner, prioritizing pixels based on the brightness, the brightness relative to all pixels, the brightness relative to all pixels in a local neighborhood, and the distance to key points introduced in previous iterations. For further details, we refer to the source code. We associate with each of these key points v its location r_v^j and color a_v^j .

A.3 Estimation of organoid barycenter and extent

We estimate the barycenter r_0^j of the organoid in an image j from the segment S_j output by the StarDist method [46] for this organoid, i.e. from a set $S_j \in \mathbb{N}_0^j$ of pixels, as $r_0^j := |S|^{-1} \sum_{s \in S} s$.

We estimate the extent σ_0^j of the organoid in an image j from the segment S_j and the set V_j

of key points (cf. Appendix A.2) as

$$\sigma_0^j = \max_{v \in V_j} \|r_v^j - r_0^j\|_2 \sup \left\{ \lambda \in \mathbb{R} \mid [r_0^j + \lambda(r_v^j - r_0^j)] \in S_j \right\} . \quad (8)$$

A.4 Motivation of assignment costs

Definition 1 We call a feasible assignment $x \in X_{V_j V_k}$ *geometrically consistent* if there exist $r^* \in \mathbb{R}^2$, $s \in \mathbb{R}^+$ and $\gamma \in [0, 2\pi)$ for which the map $f: \mathbb{R}^2 \rightarrow \mathbb{R}^2$ such that for all $r \in \mathbb{R}^2$

$$f(r) = r^* + sR_\gamma(r - r_0^j) \quad \text{with} \quad R_\gamma = \begin{pmatrix} \cos \gamma & -\sin \gamma \\ \sin \gamma & \cos \gamma \end{pmatrix} \quad (9)$$

has the following properties:

$$f(r_0^j) = r_0^k \quad (10)$$

$$\forall r \in \mathbb{R}^2: \quad |f(r) - r_0^k| = |r - r_0^j| \sigma_0^k / \sigma_0^j \quad (11)$$

$$\forall (v, w) \in x^{-1}(1): \quad f(r_v^j) = r_w^k . \quad (12)$$

Lemma 1 For any geometrically consistent $x \in X_{V_j V_k}$ and any r^*, s, γ according to Definition 1, we have $r^* = r_0^k$ and $s = \sigma_0^k / \sigma_0^j$.

PROOF By (10), $r^* = r_0^k$. Together with $s > 0$ follows $|f(r) - r_0^k| = |r^* + sR_\gamma(r - r_0^j) - r_0^k| = s|r - r_0^j|$. Together with (11) follows $s = \sigma_0^k / \sigma_0^j$. \square

Lemma 2 (Motivation of d'_{vw} and $d''_{vwv'w'}$) Let $x \in X_{V_j V_k}$ be geometrically consistent. 1. For any pair $(v, w) \in V_j \times V_k$ with $x_{vw} = 1$, we have $d'_{vw} = 0$. 2. For any distinct $v, v' \in V_j$ and any distinct $w, w' \in V_k$ such that $x_{vw} = x_{v'w'} = 1$, we have $d''_{vwv'w'} = 0$.

PROOF Firstly, $\sigma_w^k = |r_w^k - r_0^k| / \sigma_0^k = |f(r_v^j) - r_0^k| / \sigma_0^k = |r_v^j - r_0^j| / \sigma_0^j = \sigma_v^j$. Thus, $d'_{vw} = |\sigma_v^j - \sigma_w^k| = 0$. Secondly, $\alpha_{v'w'}^k = \angle(r_{v'}^k, r_w^k, r_{w'}^k - r_0^k) = \angle(f(r_v^j) - r_0^k, f(r_w^j) - r_0^k) = \angle(sR_\gamma(r_v^j - r_0^j), sR_\gamma(r_w^j - r_0^j)) = \angle(r_v^j - r_0^j, r_w^j - r_0^j) = \alpha_{vw}^j$. Thus, $d''_{vwv'w'} = |\alpha_{vw}^j - \alpha_{v'w'}^k| = 0$. \square

Lemma 3 (Bound on cost) For any instance of the partial quadratic assignment problem as defined above and any feasible solution x , we have $-(1 - \lambda)(\theta\delta + (1 - \theta)\delta') - \lambda\delta'' \leq \varphi_{c^{jk}}(x)$. For any solution x^* , also $\varphi_{c^{jk}}(x^*) \leq 0$.

PROOF Obviously, $\varphi_{\bar{c}^{jk}}(\bar{x}) \leq \varphi_{c^{jk}}(x)$ if three conditions hold: Firstly, \bar{x} is such that $\bar{x}_{vw} = 1$ for n_1^{jk} many point pairs $(v, w) \in V_j \times V_k$. Secondly, \bar{c}^{jk} is such that for all $(v, w) \in V_j \times V_k$ with $x_{vw} = 1$, \bar{c}_{vw}^{jk} is maximally negative. This happens if and only if $d_{vw} = d'_{vw} = 0$, i.e. if $\bar{c}_{vw}^{jk} = -\theta\delta - (1 - \theta)\delta'$. Thirdly, \bar{c}^{jk} is such that for all distinct $v, v' \in V_j$ and all distinct $w, w' \in V_k$, $\bar{c}_{vwv'w'}^{jk}$ is maximally negative. This happens if and only if $d''_{vwv'w'} = 0$, i.e. if $\bar{c}_{vwv'w'}^{jk} = -\delta''$. In this case, $\varphi_{\bar{c}^{jk}}(\bar{x}) = -(1 - \lambda)(\theta\delta + (1 - \theta)\delta') - \lambda\delta''$, by definition of n_1^{jk} and n_2^{jk} .

The feasible solution $0 \in X_{V_j V_k}$ is such that $\varphi_{c^{jk}}(0) = 0$. This implies for any solution x^* that $\varphi_{c^{jk}}(x^*) \leq 0$. \square

A.5 Additional qualitative experiments

In order to report, qualitatively, the clustering of a larger collection of organoid images by the methods under examination, we show in Figure 8 the set *Unlabeled-1000* of 1000 organoid images, in Figure 9 the correlation clustering of these images with respect to costs defined by the twin network learned with data augmentation, and in Figure 10 the correlation clustering of *Unlabeled-1000* with respect to costs defined by local solutions to the partial quadratic assignment problem. It can be seen from these figures that correlation clustering with respect to costs defined by local solutions to the partial quadratic assignment problem leads to more and smaller clusters.

A.6 Runtimes

Partial quadratic assignment problem. We report in Figure 11 the runtimes of the local search algorithm for the partial quadratic assignment problem, for all instances from *Test-100*. For every number $|V_j|$ of key points in the first image, the runtime is shown for the maximum number $\max |V_k|$ of key points in the second image, the average $\text{avg} |V_k|$ and the minimum

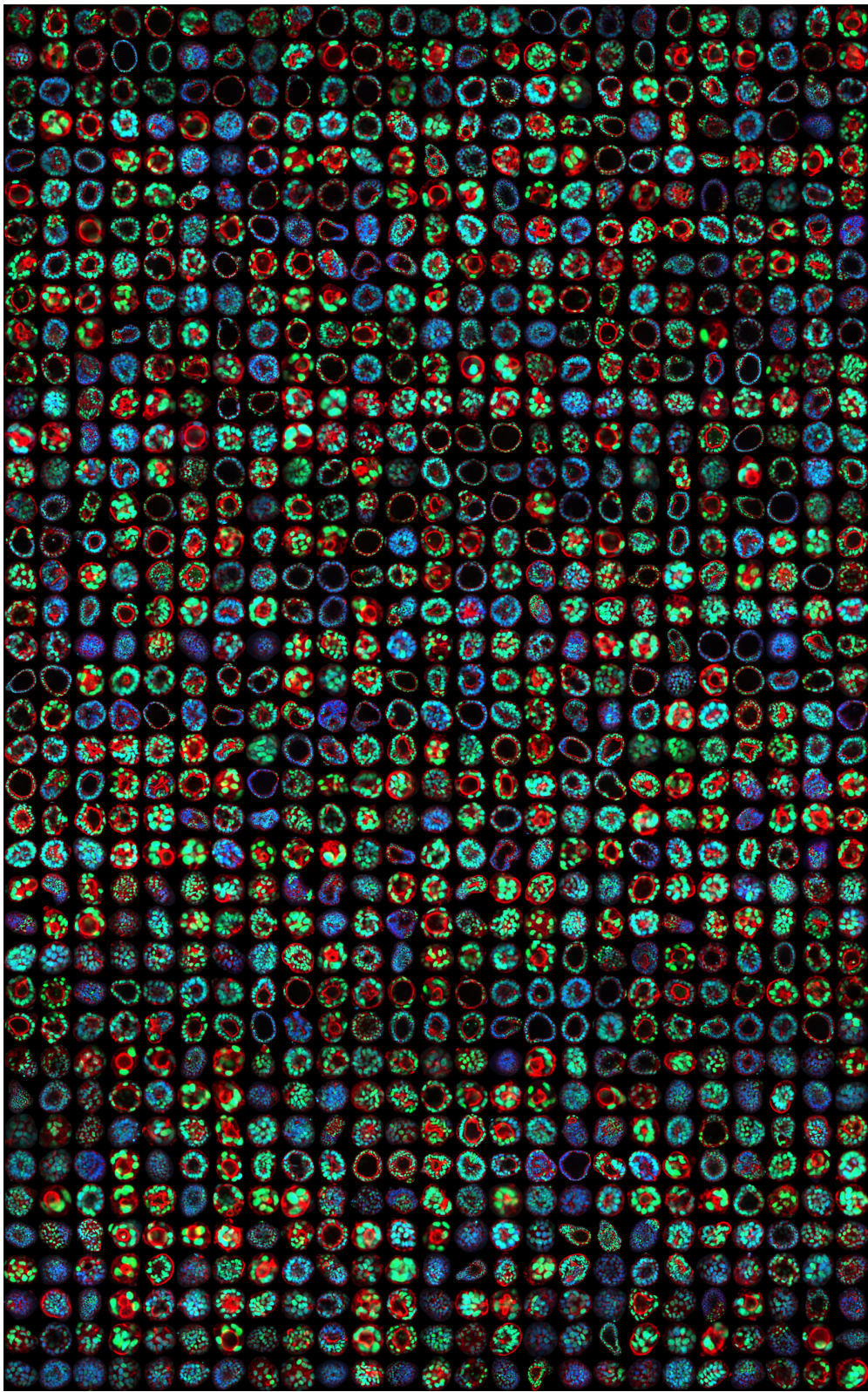


Figure 8: Depicted above is the set *Unlabeled-1000* of 1000 organoid images.

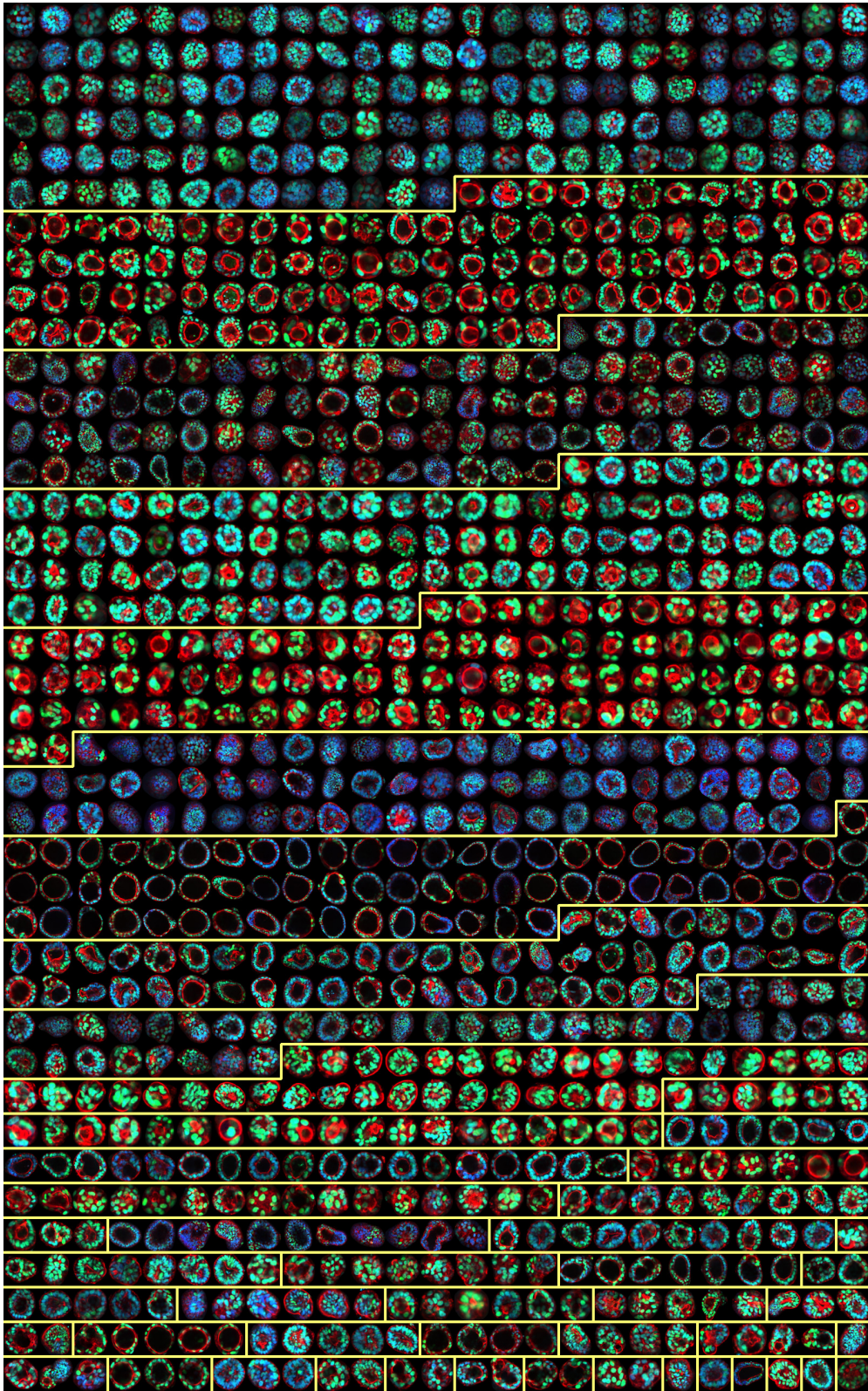


Figure 9: Depicted above is the correlation clustering of the set *Unlabeled-1000* with respect to costs defined by the twin network learned with data augmentation.

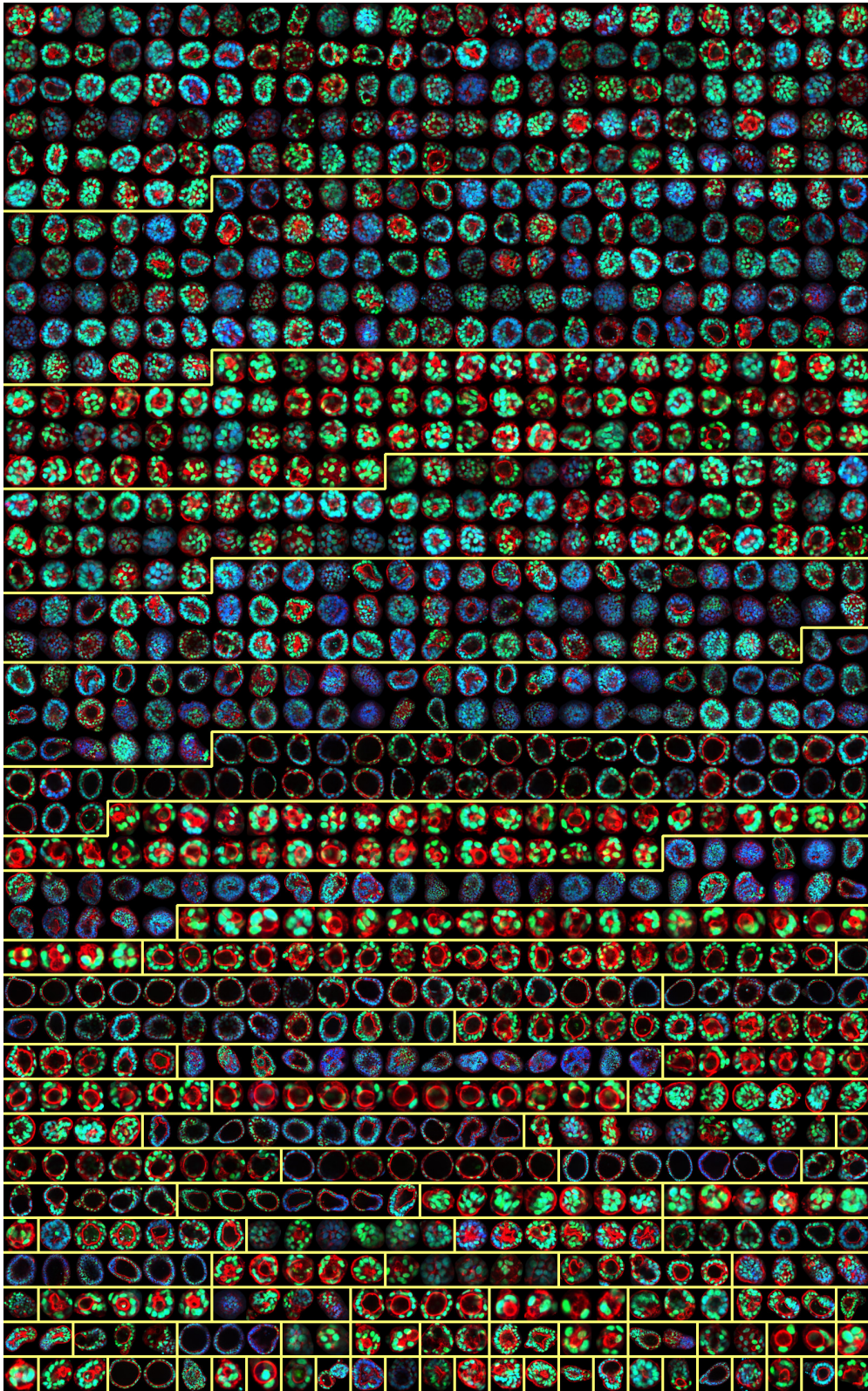


Figure 10: Depicted above is the correlation clustering of the set *Unlabeled-1000* with respect to costs defined by local solutions to the partial quadratic assignment problem.

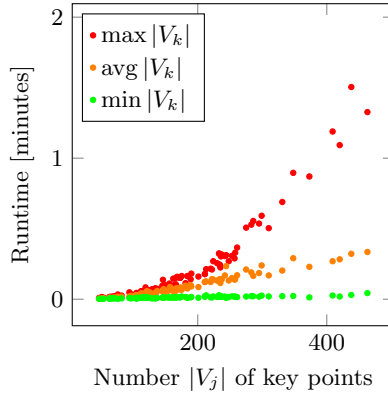


Figure 11: Reported above are the runtimes of the local search algorithm for the partial quadratic assignment problem, for all instances from *Test-100*. For every number $|V_j|$ of key points in the first image, the runtime is shown for the maximum number $\max |V_k|$ of key points in the second image, the average $\text{avg } |V_k|$ and the minimum $\min |V_k|$.

$\min |V_k|$. These runtimes are observed on a single core of an Intel Xeon Platinum 8470 CPU equipped with 512 GB of RAM, operating at 2.00 GHz.

In order to adjust the five parameters $\delta, \delta', \delta'', \theta$ and λ of the instances of the partial quadratic assignment problem, we performed simulated annealing for 8 hours on one core of the same CPU.

Correlation clustering problem. All instances of the correlation clustering problem have been solved to optimality using Gurobi on all 52 cores of the same CPU. For costs defined by the twin network with images as input, this has taken at most 20 minutes. For costs defined by the twin network with histograms as input, it has taken at most 42 minutes. For costs defined by local solutions to the partial quadratic assignment problem, it has taken at most 14 minutes. For costs based on the Hellinger distance, it has taken at most 73 minutes.

Twin networks. Learning the twin network with images as input, for 6,000 iterations, takes about 20 minutes; learning the twin network with histograms as input, for 6,000 iterations, takes about 70 minutes, both on a single NVIDIA GeForce RTX 4900.

A.7 Ethical considerations

This article presents work whose goal is to advance the fields of computer vision and biomedical image analysis. There are many potential societal consequences of this work, none which we feel must be specifically highlighted here.

The H9 human embryonic stem cell (hESC) line was purchased from WiCell, and GFP reporter for PDX1 was generated in the Grapin-Botton lab. Approval to work on hESCs was obtained from the Robert Koch Institute under reference number 3.04.02/0148, and the hESC work was conducted according to the guidelines. Pancreatic organoids were generated using hESC-derived pancreatic progenitors, as previously reported [18].

References

- [1] A. Abbas and P. Swoboda. FastDOG: Fast discrete optimization on GPU. In *CVPR*, 2022. doi:10.1109/CVPR52688.2022.00053.
- [2] A. Abbas and P. Swoboda. RAMA: A rapid multicut algorithm on GPU. In *CVPR*, 2022. doi:10.1109/CVPR52688.2022.00802.
- [3] A. Abbas and P. Swoboda. ClusterFuG: clustering fully connected graphs by multicut. In *ICML*, 2023. doi:10.5555/3618408.3618410.
- [4] A. Abbas and P. Swoboda. DOGE-Train: Discrete optimization on GPU with end-to-end training. In *AAAI*, 2024.
- [5] A. Alush and J. Goldberger. Hierarchical image segmentation using correlation clustering. *Transactions on Neural Networks and Learning Systems*, 27(6):1358–1367, 2016. doi:10.1109/TNNLS.2015.2505181.
- [6] B. Andres, J. H. Kappes, T. Beier, U. Köthe, and F. A. Hamprecht. Probabilistic image segmentation with closedness constraints. In *ICCV*, 2011. doi:10.1109/ICCV.2011.6126550.

- [7] P. Arabie and S. A. Boorman. Multidimensional scaling of measures of distance between partitions. *Journal of Mathematical Psychology*, 10(2):148–203, 1973. doi:10.1016/0022-2496(73)90012-6.
- [8] N. Bansal, A. Blum, and S. Chawla. Correlation clustering. *Machine Learning*, 56(1):89–113, 2004. doi:10.1023/B:MACH.0000033116.57574.95.
- [9] K. Bhatia, H. Jain, P. Kar, M. Varma, and P. Jain. Sparse local embeddings for extreme multi-label classification. In *NeurIPS*, 2015. URL: https://proceedings.neurips.cc/paper_files/paper/2015/file/35051070e572e47d2c26c241ab88307f-Paper.pdf.
- [10] L. Bourdev and J. Malik. Poselets: Body part detectors trained using 3D human pose annotations. In *ICCV*, 2009. doi:10.1109/ICCV.2009.5459303.
- [11] C. Brémond Martin, C. Simon Chane, C. Clouchoux, and A. Histace. Recent trends and perspectives in cerebral organoids imaging and analysis. *Frontiers in Neuroscience*, 15, 2021. doi:10.3389/fnins.2021.629067.
- [12] E. Cela. *The quadratic assignment problem: theory and algorithms*. Springer, 2013. doi:10.1007/978-1-4757-2787-6.
- [13] D. Chicco. Siamese neural networks: An overview. In H. Cartwright, editor, *Artificial Neural Networks*, pages 73–94. Springer, 2021. doi:10.1007/978-1-0716-0826-5_3.
- [14] M. Cho, K. Alahari, and J. Ponce. Learning graphs to match. In *ICCV*, 2013. doi:10.1109/ICCV.2013.11.
- [15] E. D. Demaine, D. Emanuel, A. Fiat, and N. Immerlica. Correlation clustering in general weighted graphs. *Theoretical Computer Science*, 361(2–3):172–187, 2006. doi:10.1016/j.tcs.2006.05.008.
- [16] T. Dłask and B. Savchynskyy. Relative-interior solution for (incomplete) linear assignment problem with applications to quadratic assignment problem. *arXiv preprint*, 2023. doi:10.48550/arXiv.2301.11201.
- [17] L. Fillioux, E. Gontran, J. Cartry, J. R. Mathieu, S. Bedja, A. Boilève, P.-H. Cournède, F. Jaulin, S. Christodoulidis, and M. Vakalopoulou. Spatio-temporal analysis of patient-derived organoid videos using deep learning for the prediction of drug efficacy. In *ICCV Workshops*, 2023. doi:10.1109/ICCVW60793.2023.00425.
- [18] C. Gonçalves, M. Larsen, S. Jung, J. Stratmann, A. Nakamura, M. Leuschner, L. Hersemann, R. Keshara, S. Perlman, L. Lundvall, L. Thuesen, K. Hare, I. Amit, A. Jørgensen, Y. Kim, A. del Sol, and A. Grapin-Botton. A 3D system to model human pancreas development and its reference single-cell transcriptome atlas identify signaling pathways required for progenitor expansion. *Nature Communications*, 12, 2021. doi:10.1038/s41467-021-23295-6.
- [19] A. Grapin-Botton and Y. H. Kim. Pancreas organoid models of development and regeneration. *Development*, 149(20):dev201004, 2022. doi:10.1242/dev.201004.
- [20] Gurobi Optimization, LLC. Gurobi Optimizer Reference Manual, 2023. URL: <https://www.gurobi.com>.
- [21] S. Haller, L. Feineis, L. Hutschenreiter, F. Bernard, C. Rother, D. Kainmüller, P. Swoboda, and B. Savchynskyy. A comparative study of graph matching algorithms in computer vision. In *ECCV*, 2022. doi:10.1007/978-3-031-20050-2_37.
- [22] K. He, X. Zhang, S. Ren, and J. Sun. Deep residual learning for image recognition. In *CVPR*, 2016. doi:10.1109/CVPR.2016.90.
- [23] E. Hellinger. Neue Begründung der Theorie quadratischer Formen von unendlichvielen Veränderlichen. *Journal für die reine und angewandte Mathematik*, 1909(136):210–271, 1909. doi:10.1515/crll.1909.136.210.
- [24] K. Ho, A. Chatzimichailidis, M. Keuper, and J. Keuper. MSM: Multi-stage multicuts for scalable image clustering. In *High Performance Computing*, 2021. doi:10.1007/978-3-030-90539-2_18.

- [25] M. Huch, J. A. Knoblich, M. P. Lutolf, and A. Martinez-Arias. The hope and the hype of organoid research. *Development*, 144(6):938–941, 2017. doi:10.1242/dev.150201.
- [26] L. Hutschenreiter, S. Haller, L. Feineis, C. Rother, D. Kainmüller, and B. Savchynskyy. Fusion moves for graph matching. In *ICCV*, 2021. doi:10.1109/ICCV48922.2021.00621.
- [27] R. Jovanovic, A. P. Sanfilippo, and S. Voß. Fixed set search applied to the clique partitioning problem. *European Journal of Operational Research*, 309(1):65–81, 2023. doi:10.1016/j.ejor.2023.01.044.
- [28] J. H. Kappes, P. Swoboda, B. Savchynskyy, T. Hazan, and C. Schnörr. Multicuts and perturb & MAP for probabilistic graph clustering. *Journal of Mathematical Imaging and Vision*, 56(2):221–237, 2016. doi:10.1007/S10851-016-0659-3.
- [29] R. Keshara, Y. H. Kim, and A. Grapin-Botton. Organoid imaging: Seeing development and function. *Annual Review of Cell and Developmental Biology*, 38(1):447–466, 2022. doi:10.1146/annurev-cellbio-120320-035146.
- [30] M. Keuper, E. Levinkov, N. Bonneel, G. Lavoué, T. Brox, and B. Andres. Efficient decomposition of image and mesh graphs by lifted multicuts. In *ICCV*, 2015. doi:10.1109/ICCV.2015.204.
- [31] M. A. Lancaster and J. A. Knoblich. Organogenesis in a dish: modeling development and disease using organoid technologies. *Science*, 345(6194):1247125, 2014. doi:10.1126/science.1247125.
- [32] E. L. Lawler. The quadratic assignment problem. *Management science*, 9(4):586–599, 1963. doi:10.1287/mnsc.9.4.586.
- [33] B. H. Lee, I. Seijo-Barandiaran, and A. Grapin-Botton. Epithelial morphogenesis in organoids. *Current Opinion in Genetics & Development*, 72:30–37, 2022. doi:10.1016/j.gde.2021.10.001.
- [34] A. Lewis, R. Keshara, Y. H. Kim, and A. Grapin-Botton. Self-organization of organoids from endoderm-derived cells. *Journal of Molecular Medicine*, 99(4):449–462, 2021. doi:10.1007/s00109-020-02010-w.
- [35] I. Loshchilov and F. Hutter. Decoupled weight decay regularization. In *ICLR*, 2019. URL: <https://openreview.net/forum?id=Bkg6RiCqY7>.
- [36] I. Lukonin, M. Zinner, and P. Liberali. Organoids in image-based phenotypic chemical screens. *Experimental & Molecular Medicine*, 53(10):1495–1502, 2021. doi:10.1038/s12276-021-00641-8.
- [37] F. Marra, G. Poggi, C. Sansone, and L. Verdoliva. Correlation clustering for PRNU-based blind image source identification. In *International Workshop on Information Forensics and Security*, 2016. doi:10.1109/WIFS.2016.7823910.
- [38] J. M. Matthews, B. Schuster, S. S. Kashaf, P. Liu, R. Ben-Yishay, D. Ishay-Ronen, E. Izumchenko, L. Shen, C. R. Weber, M. Bielski, S. S. Kupfer, M. Bilgic, A. Rzhetsky, and S. Tay. OrganoID: A versatile deep learning platform for tracking and analysis of single-organoid dynamics. *PLOS Computational Biology*, 18(11):1–16, 2022. doi:10.1371/journal.pcbi.1010584.
- [39] M. Meilă. Comparing clusterings—an information based distance. *Journal of Multivariate Analysis*, 98(5):873–895, 2007. doi:10.1016/j.jmva.2006.11.013.
- [40] J. Min, J. Lee, J. Ponce, and M. Cho. Spair-71k: A large-scale benchmark for semantic correspondence. *arXiv preprint*, 2019. doi:10.48550/arXiv.1908.10543.
- [41] T. Park, T. K. Kim, Y. D. Han, K.-A. Kim, H. Kim, and H. S. Kim. Development of a deep learning based image processing tool for enhanced organoid analysis. *Scientific Reports*, 13(1), 2023. doi:10.1038/s41598-023-46485-2.
- [42] W. M. Rand. Objective criteria for the evaluation of clustering methods. *Journal of the American Statistical Association*, 66(336):846–850, 1971. doi:10.1080/01621459.1971.10482356.

- [43] M. Rolínek, P. Swoboda, D. Zietlow, A. Paulus, V. Musil, and G. Martius. Deep graph matching via blackbox differentiation of combinatorial solvers. In *ECCV*, 2020. doi:10.1007/978-3-030-58604-1_25.
- [44] G. Rossi, A. Manfrin, and M. P. Lutolf. Progress and potential in organoid research. *Nature Reviews Genetics*, 19(11):671–687, 2018. doi:10.1038/s41576-018-0051-9.
- [45] R. Rouhi, F. Bertini, and D. Montesi. User profiles’ image clustering for digital investigations. *Forensic Science International: Digital Investigation*, 38:301171, 2021. doi:10.1016/j.fsidi.2021.301171.
- [46] U. Schmidt, M. Weigert, C. Broaddus, and G. Myers. Cell detection with star-convex polygons. In *MICCAI*, 2018. doi:10.1007/978-3-030-00934-2_30.
- [47] M. M. Sørensen. A separation heuristic for 2-partition inequalities for the clique partitioning problem. Technical report, 2020. URL: <https://optimization-online.org/wp-content/uploads/2020/07/7917.pdf>.
- [48] M. M. Sørensen and A. N. Letchford. CP-Lib: Benchmark instances of the clique partitioning problem. *Mathematical Programming Computation*, 16(1):93–111, 2023. doi:10.1007/s12532-023-00249-1.
- [49] P. Swoboda, B. Andres, A. Hornakova, F. Bernard, J. Iрмаi, P. Roetzer, B. Savchynskyy, D. Stein, and A. Abbas. Structured prediction problem archive. *arXiv preprint*, 2023. doi:10.48550/arXiv.2202.03574.
- [50] P. Swoboda, D. Kainmüller, A. Mokarian, C. Theobalt, and F. Bernard. A convex relaxation for multi-graph matching. In *CVPR*, 2019. doi:10.1109/CVPR.2019.01141.
- [51] P. Swoboda, C. Rother, H. A. Alhaija, D. Kainmüller, and B. Savchynskyy. A study of lagrangean decompositions and dual ascent solvers for graph matching. In *CVPR*, 2017. doi:10.1109/CVPR.2017.747.
- [52] L. Torresani, V. Kolmogorov, and C. Rother. Feature correspondence via graph matching: Models and global optimization. In *ECCV*, 2008. doi:10.1007/978-3-540-88688-4_44.
- [53] S. Tourani, C. Rother, M. H. Khan, and B. Savchynskyy. Unsupervised deep graph matching based on cycle consistency. *arXiv preprint*, 2023. doi:10.48550/ARXIV.2307.08930.
- [54] N. Veldt. Correlation clustering via strong triadic closure labeling: Fast approximation algorithms and practical lower bounds. In *ICML*, 2022. URL: <https://proceedings.mlr.press/v162/veldt22a.html>.
- [55] J. Wang, F. Zhou, S. Wen, X. Liu, and Y. Lin. Deep metric learning with angular loss. In *ICCV*, 2017. doi:10.1109/ICCV.2017.283.